Soft Matter

PAPER

View Article Online
View Journal | View Issue

Cite this: *Soft Matter*, 2015, 11, 6968

Magnetophoresis of superparamagnetic nanoparticles at low field gradient: hydrodynamic effect†

Sim Siong Leong,[a] Zainal Ahmad[a] and JitKang Lim*[ab]

Convective current driven by momentum transfer between magnetic nanoparticles (MNPs) and their surrounding fluid during magnetophoresis process under a low gradient magnetic field (<100 T m^{-1}) is presented. This magnetophoresis induced convective flow, which imposed direct hydrodynamic effects onto the separation kinetics of the MNPs under low gradient magnetic separation (LGMS), is analogous to the natural convection found in heat transportation. Herein, we show the significance of the induced convection in controlling the transport behavior of MNPs, even at a very low particle concentration of 5 mg L^{-1}, and this feature can be characterized by the newly defined magnetic Grashof number. By incorporating fluid flow equations into the existing magnetophoresis model, we reveal two unique features of this convective flow associated with low gradient magnetophoresis, namely, (1) the continuous homogenization of the MNPs solution and (2) accompanying sweeping flow that accelerates the collection of MNPs. According to both simulation and experimental data, the induced convection boosts the magnetophoretic capture of MNPs by approximately 30 times compared to the situation with no convection.

Received 9th June 2015,
Accepted 21st July 2015

DOI: 10.1039/c5sm01422k

www.rsc.org/softmatter

1 Introduction

In recent years, magnetic nanoparticles (MNPs) have emerged as one of the most versatile nanomaterials with huge potential for various biomedical[1–6] and environmental applications.[7–11] For separation processes, MNPs are used in the following way: surface-functionalized MNPs are initially dispersed into a solution containing targeting compounds; thus, the MNPs can be tagged onto the aforementioned compounds either through specific or non-specific binding. Subsequently, the MNP-tagged compounds are withdrawn from the solution or directed to a specific region in a controlled manner by an externally applied magnetic field.[12] This scheme allows the separation of non-magnetic compounds by a process known as magnetophoresis, which involves the controlled motion of MNPs under an externally applied magnetic field relative to the surrounding fluid.[13]

There are numerous benefits associated to the use of MNPs in promoting the separation of biological components as compared to conventional separation processes.[14] However, because MNPs are extremely small, their collection from the surrounding media poses a great challenge due to the significant perturbation of their magnetophoretic pathway by thermal energy and viscous drag.[15] Therefore, high gradient magnetic field is applied for the MNPs to attain a large magnetophoretic force to overcome the randomization energy and opposing force(s) and achieve separation in a reasonable time scale. This process is known as high gradient magnetic separation (HGMS),[16] and it encounters four significant drawbacks: (1) high purchase and installation cost;[17] (2) complexity in developing analytical solutions due to the highly inhomogeneous magnetic field inside the HGMS column;[16] (3) high tendency of MNP deposition on the wires within the HGMS column, which causes reduction in separation efficiency or even brings about permanent retention of MNPs in the column;[14] and (4) energy losses due to the Joule effect during the magnetization and demagnetization of magnetizable wires.[18]

[a] *School of Chemical Engineering, Universiti Sains Malaysia, Nibong Tebal, Penang 14300, Malaysia. E-mail: chjitkangl@usm.my*
[b] *Department of Physics, Carnegie Mellon University, Pittsburgh, PA 15213, USA*

† Electronic supplementary information (ESI) available: S1 provides the justification for the validity of the Beer–Lambert law in this study. S2 illustrates the calculation to justify that the amount of MB overwhelms that of the MNPs in the dye-tracing experiment described in Section 2.3. S3 shows the detailed analysis of the magnetic Bjerrum length and aggregation parameter for the MNPs system employed in the current work. S4 demonstrates the magnetic flux density of the cylindrical magnet in a three dimensional space and justifies the suitability of the one dimensional magnetic flux density approximation in the current work. S5 and S6 give a more detailed description of the simulation of the non MNPs/fluid interacting magnetophoresis model and hydrodynamically interacting magnetophoresis model, respectively, by providing a discussion on the initial and boundary conditions involved in the simulation. S7 provides a list of the symbols used in the current work together with their units. The supplementary video serves to give a clearer illustration of the difference between the simulation results from the both models developed in this work. See DOI: 10.1039/c5sm01422k

Recently, Yavuz and co-workers demonstrated the feasibility of low gradient magnetic fields generated by a permanent magnet (magnetic flux density gradient $\nabla B < 100\ \mathrm{T\ m^{-1}}$) in the collection of 4 nm superparamagnetic magnetite nanocrystals.[19] Successful implementation of this separation method, which is known as low gradient magnetic separation (LGMS), was identified to be because of the formation of field-induced aggregates.[12,19] This reversible aggregation has greatly altered the dynamic behavior of LGMS by accelerating MNP collection and reducing separation time. Due to its simplicity and cost-effectiveness,[17] many current research efforts are dedicated to study the underlying principles that define the transport behavior of MNPs under LGMS.[20–26] By taking the interparticle interaction between MNPs (which is known as MNPs/MNPs interaction in this article) into consideration, motion of MNPs under LGMS has been described quantitatively to predict the kinetic profile of their separation.[12,20,21,25] Furthermore, the morphology of MNP aggregation under LGMS has been investigated and explained by including magnetic interaction into the classical Derjaguin–Landau–Verwey–Overbeek (DLVO) theory.[22] Moreover, the transient behavior of MNP aggregation upon the application of an external magnetic field has been studied and simulated.[24]

While MNPs/MNPs interaction has been studied comprehensively, the interaction between MNPs and surrounding fluid, which is contributed by the momentum transfer through the collision between both species, has been neglected by most researchers that have studied LGMS system.[20,21,25,26] There are very few studies that report this type of interaction, which is termed MNPs/fluid interaction in this article. Because most of the engineering applications of MNPs involve the controlled magnetophoretic movement of MNPs suspended in fluid,[5,6,8,9,27–29] it is reasonable to hypothesize that the MNPs/fluid interaction is inevitable and it plays an essential role in dictating the LGMS kinetics. Microscopically, the magnetophoretic separation of MNPs in microfluidic systems, where MNPs experience a highly localized magnetic field gradient, has been studied and simulated theoretically by taking the MNPs/fluid interaction into consideration.[30–34] From the studies of Furlani and coworkers on microfluidic systems, it was observed that the local fluid flow is heavily influenced by the magnetophoretic motion of MNPs,[32] which makes us to believe that the MNPs/fluid interaction also has a pronounced effect on the LGMS process. However, there is almost no discussion on the macroscopic effect of the MNPs/fluid interaction on LGMS, which is widely utilized in various engineering applications. In conjunction with this situation, we intend to complete the physical understanding on the magnetophoretic behavior of MNPs under LGMS by investigating how the MNPs/fluid interaction influences LGMS performance.

In this study, a dilute MNPs solution was utilized such that the MNPs/MNPs interaction is negligible and can be safely ignored in the analysis of the result. Initially, a magnetophoresis experiment was conducted to study the kinetic behavior of a MNPs solution subjected to a low gradient magnetic field. Subsequently, two different models were developed to describe the low gradient magnetophoresis of MNPs. In the first model, the classical assumption was made that the motion of MNPs is solely governed by magnetic, gravitational and Brownian forces, as well as viscosity, while the fluid remains stagnant and unaltered by the MNPs motion at all times. Later, in the second model, the drift-diffusion equation was coupled and solved together with fluid flow equations with the assumption that the surrounding fluid of the MNPs is no longer stagnant but can be perturbed by the motion of MNPs. The simulation results from both models were compared with experimental results to justify the importance of hydrodynamic effect that originates from the MNPs/fluid interaction in dictating the LGMS process. Furthermore, the magnetic Grashof number was developed to characterize the significance of magnetophoresis induced convection under LGMS in a dimensionless form.

2 Experimental section

2.1 Characterization of magnetic nanoparticles (MNPs)

Transmission electron microscopy (TEM). MNPs solution used in this experiment was purchased from Ocean NanoTech, consisting of an aqueous suspension of iron oxide nanoparticles coated with polyethylene glycol (PEG). TEM was used to capture the images of the MNPs. The captured images enabled us to determine the geometrical shape and magnetic core size of MNPs. A droplet of dilute MNPs solution ($\sim$20 mg $\mathrm{L^{-1}}$) was deposited and dried on a carbon grid for 30 minutes. The dried MNPs, which were immobilized on the carbon grid, were observed using TEM (JEOL, JEM-20CX).

Dynamic light scattering (DLS). DLS technique was employed to determine the hydrodynamic size of MNPs.[35] Before conducting DLS analysis, the as-received MNPs solution was diluted to 10 mg $\mathrm{L^{-1}}$ so that the effects of multiple scattering and particle interaction were minimized during the measurement. The fluctuation of the scattered light intensity was detected and measured at an angle of 173° to the incident light (Malvern Instruments Zetasizer ZS). The transient light intensity fluctuation was fitted into a correlation function that decayed exponentially with time. The correlation function decayed more rapidly for smaller MNPs as light intensity fluctuation is greater due to the faster diffusion of small MNPs. the cumulants method was employed to analyze the correlation function so that the translational diffusivity of MNPs suspended in a solution is obtained. Subsequently, according to the translational diffusivity of MNPs, the hydrodynamic size of the MNPs was inferred using the Einstein–Stokes equation. Therefore, in this analysis, all the MNPs were assumed to be spherical in shape.

Vibrating sample magnetometer (VSM). VSM was used to characterize the magnetic response of MNPs. To conduct the VSM measurement, 0.0006 g of MNPs was dispersed in an epoxy, thus forming a cast epoxy sample. The cast epoxy sample was attached to a vibrating glass rod placed at the center of an electromagnetic direct current (DC) field. The magnetic response of the sample was measured with a full sweep for both the positive and negative field components with digitally controlled field stepping and data averaging.

2.2 Magnetophoresis kinetics measurement

The experimental setup is illustrated in Fig. 1. A standard 1 × 1 × 4 cm disposable cuvette was filled with 3 mL of homogeneous MNPs solution such that the solution surface measured 3 cm vertically from the base of the cuvette. Subsequently, the cuvette was placed on top of a cylindrical neodymium boron ferrite (NdFeB) magnet. The NdFeB magnet was N50-graded with the remanent magnetization of 1.45 T and was obtained from Ningbo YuXiang E&M Int'l Co, Ltd. A UV-vis spectrophotometer (Agilent Cary-60) was employed to measure the concentration of the MNPs in solution, where monochromatic light with the wavelength of 530 nm was passed through the MNPs solution and the light absorbance was recorded. The initial concentration of MNPs was varied, within the range from 10 to 100 mg L^{-1}, to probe the particle concentration effect on magnetophoresis kinetics. Then, the light absorbance was recorded in different locations along the cuvette so that a complete picture of magnetophoresis kinetics could be captured. Because the Beer–Lambert's law was proven to be valid for the concentration range of MNPs employed in this study (see ESI,† S1 for justification), the normalized MNPs concentration (with respect to initial concentration of MNPs solution before the magnetophoresis experiment begins) was calculated as follows:

$$c_{N,MNPs} = \frac{A - A_0}{A_i - A_0} \quad (1)$$

where A is light absorbance of the MNPs solution, A_0 is the light absorbance of the blank solution and A_i is the initial light absorbance of the MNPs solution.

2.3 Dye-tracing experiment

This experiment was performed to visually trace the fluid motion during magnetophoresis. Initially, approximately 3000 mg L^{-1} of concentrated methylene blue (MB) was introduced carefully to the bottom of a cuvette containing 3 mL of MNPs solution using a syringe. The MNPs solution was then subjected to magnetophoresis and the motion of the dye in the solution was captured. Because dye molecules are highly positively charged and MNPs have an average zeta potential of −10 mV, it is believed that some of the dye molecules might adhere to the MNPs due to electrostatic interaction.[36] However, because MB molecules are present in excess, there should be a significant amount of freely suspended dye molecules that can trace the fluid motion within the MNPs solution for visualization of magnetophoresis (see ESI,† S2 for justification). The procedure mentioned above was carried out using MNPs solutions with the following concentrations: 0 (blank solution, which was used as the control), 5, 10, 20, 50, 100 mg L^{-1}. The dye motion in the solutions with different concentrations of MNPs under magnetophoresis was compared.

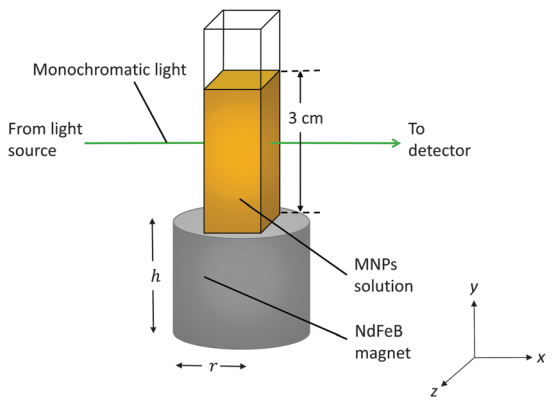

Fig. 1 Setup of magnetophoresis experiment. Initially, a cuvette was filled with a homogeneously dispersed MNPs solution and was placed on a grade N50 NdFeB cylindrical permanent magnet with the remanent magnetization of 1.45 T and the radius and height of the magnet were 0.7 cm and 1.5 cm, respectively. The light absorbance of the MNPs solution was measured every 5 minutes after magnetophoresis started using a UV-vis spectrophotometer and the result was used to infer the MNPs concentration.

3 Theoretical model

In this study, two models were developed to predict the separation kinetic profile of magnetophoresis in the experiment described above, namely, non MNPs/fluid interacting and hydrodynamically interacting magnetophoresis models. The predictions from both models were then compared with the experimental results to verify the accuracy of the models and hence justify the importance of the hydrodynamic interaction in the low gradient magnetophoresis of MNPs.

3.1 Non MNPs/fluid interacting magnetophoresis model

Several assumptions were made in the development of this model: (1) MNPs are distributed uniformly throughout the solution prior to the application of magnetic field, (2) MNPs/MNPs interaction is negligible due to the non-interactive nature of the particle system (see ESI,† S3 for justification), (3) MNPs are spherical in shape and consist of a magnetic core surrounded by a layer of non-magnetic polyethylene glycol (PEG), (4) the magnetophoretic migration of MNPs in the solution is creeping motion that obeys Stokes' law, (5) the motion of MNPs does not create any fluid flow perturbation such that the surrounding fluid remains stagnant throughout the entire course of magnetophoresis and (6) the vertical component of the magnetic flux density gradient throughout the MNPs solution, which is subjected to magnetophoresis, is far more dominant compared to its horizontal counterpart (see ESI,† S4 for more detailed justification).

Under an external magnetic field, there are four forces acting on MNPs that govern the motion of MNPs in the MNPs solution: (1) magnetic force, which is due to the response of the magnetic dipole moment in MNPs to the externally applied magnetic field; (2) viscous drag force, which is due to the resistance contributed by the relative motion of MNPs in solution; (3) gravitational force and (4) Brownian force, which induces the diffusion of MNPs along the MNPs concentration gradient and originates from thermal motion. The transport behaviour of MNPs in the fluid throughout magnetophoresis,

due to the combination of diffusion and fluid advection effects, is described by the drift-diffusion equation:[37]

$$\frac{\partial c}{\partial t} = D\nabla^2 c - \nabla \times (uc) \quad (2)$$

where c is concentration of the MNPs solution, u is magnetophoretic velocity of MNPs and D is diffusivity of MNPs in the solution, which can be calculated using Einstein–Stokes equation:[15]

$$D = \frac{k_B T}{6\pi\eta R_h} \quad (3)$$

where k_B is Boltzmann constant, T is absolute temperature, η is the dynamic viscosity of fluid and R_h is the hydrodynamic radius of the MNPs (=21.5 $\times$ 10^{-9} m). The first term on the right hand side of eqn (2) depicts the transport of MNPs in solution due to the thermal motion of particles, whereas the second term represents the divergence of MNPs flux, which is induced by magnetic, viscous and gravitational forces acting on each individual MNP during magnetophoresis. According to the Newton's second law of motion, the acceleration of MNPs, du/dt, is dependent on the sum of all forces that are acting on it:

$$m_p \frac{du}{dt} = F_{mag} + F_d + F_g \quad (4)$$

where m_p is mass of an MNP, F_{mag} is magnetic force, F_d is viscous drag force and F_g is gravitational force. The inertial term $\left(m_p \frac{du}{dt}\right)$ is negligible under low Reynold number flow, and hence for simplicity, it is neglected in the present analysis.[37] Based on this assumption, eqn (4) finally turns out to be

$$0 = F_{mag} + F_d + F_g \quad (5)$$

The magnetic force F_{mag} acting on an MNP is formulated as follows:[12]

$$F_{mag} = \mu \nabla B \quad (6)$$

where μ is magnetic dipole moment and B is magnetic flux density. For an axially magnetized cylindrical magnet, the magnetic flux density along the axis of the magnet, where vertical distance from the magnet pole face is given by y, can be calculated as follows:[38]

$$B = \frac{B_r}{2}\left[\frac{y+h}{\sqrt{(y+h)^2 + r^2}} - \frac{y}{\sqrt{y^2 + r^2}}\right] \quad (7)$$

where B_r is remanent magnetic flux density, h is the height of cylindrical magnet and r is the radius of cylindrical magnet. We assume that the variation of magnetic flux density along the radial direction is insignificant compared to that of the axial direction (Assumption 6), x- and z-components of ∇B are negligible and ∇B can thus be approximated as follows:

$$\nabla B \approx \frac{\partial B}{\partial y}\boldsymbol{e}_y = \frac{B_r r^2}{2}\left[\frac{1}{\left[(y+h)^2 + r^2\right]^{\frac{3}{2}}} - \frac{1}{[y^2 + r^2]^{\frac{3}{2}}}\right]\boldsymbol{e}_y \quad (8)$$

where $\boldsymbol{e}_y$ is the unit vector pointing to the positive y-direction. On the other hand, magnetic dipole moment is given as follows:

$$\mu = m_p M_{p,m} \quad (9)$$

where $M_{p,m}$ is the mass magnetization of MNPs, which is the function of magnetic field strength, H, that is applied. The relationship between the mass magnetization of MNPs and the applied magnetic field strength can be obtained by fitting the magnetization curve, which is obtained from VSM, to the following equation:[39]

$$M_{p,m} = M_s L\left(\frac{mH}{k_B T}\right) = M_s\left[\coth\left(\frac{mH}{k_B T}\right) - \frac{k_B T}{mH}\right] \quad (10)$$

where M_s is the saturation magnetization per unit mass of MNPs, m is the strength of the magnetic moment for one magnetic dipole and L is the Langevin function [$L(x)$ = coth(x) $-$ 1/x]. Because the relative permeability of water approaches unity, the relationship between magnetic flux density and magnetic field strength in the aqueous MNPs solution is given as follows:

$$B = \mu_0 H \quad (11)$$

By inserting eqn (7)–(11) into eqn (6), the magnetic force acting on a MNP can be expressed as a function of distance (along the axial or vertical direction, y) from the magnet pole as follows:

$$F_{mag} = \left(m_p M_s L\left\{\frac{mB_r}{2\mu_0 k_B T}\left[\frac{y+h}{\sqrt{(y+h)^2 + r^2}} - \frac{y}{\sqrt{y^2 + r^2}}\right]\right\} \times \frac{B_r r^2}{2}\left[\frac{1}{\left[(y+h)^2 + r^2\right]^{\frac{3}{2}}} - \frac{1}{[y^2 + r^2]^{\frac{3}{2}}}\right]\right)\boldsymbol{e}_y \quad (12)$$

The viscous drag force experienced by an MNP that is moving in a viscous fluid (or under low Reynold number environment) is formulated by Stokes' law, which is given as follows:[25]

$$F_d = -6\pi\eta r_h u = -6\pi\eta R_h(u_x e_x + u_y e_y + u_z e_z) \quad (13)$$

where u_x, u_y and u_z are x-, y- and z-components of MNPs magnetophoretic velocity, respectively. Moreover, $\boldsymbol{e}_x$ and $\boldsymbol{e}_z$ are the unit vectors pointing to the positive x- and z-directions.

The gravitational force acting on a MNP is given by the Newton's law of gravitation:

$$F_g = -m_p \boldsymbol{g} = -m|\boldsymbol{g}|\boldsymbol{e}_y \quad (14)$$

where $\boldsymbol{g}$ is gravitational acceleration vector and $|\boldsymbol{g}|$ is the magnitude of gravitational acceleration ($\approx$9.81 m s^{-2} on Earth surface).

By incorporating eqn (12)–(14) in eqn (5), eqn (15) are obtained. Upon rearrangement, the x-, y- and z-components of magnetophoretic velocity of MNPs subjected to magnetophoresis in the model system are given by eqn (16).

Eqn (16) are required to solve eqn (2) to predict the transient behavior and generate a separation kinetic profile of the magnetophoresis process. (Please refer to ESI,† S5 for details

of the computer simulation, including the initial and boundary conditions employed in this model).

$$-6\pi\eta r_{\mathrm{h}} u_x = 0 \tag{15a}$$

$$\left(m_{\mathrm{p}} M_{\mathrm{s}} L \left\{ \frac{m B_{\mathrm{r}}}{2\mu_0 k_{\mathrm{B}} T} \left[\frac{y+h}{\sqrt{(y+h)^2 + r^2}} - \frac{y}{\sqrt{y^2 + r^2}} \right] \right\} \times \frac{B_{\mathrm{r}} r^2}{2} \left[\frac{1}{\left[(y+h)^2 + r^2\right]^{\frac{3}{2}}} - \frac{1}{[y^2 + r^2]^{\frac{3}{2}}} \right] \right) - m_{\mathrm{p}}|\boldsymbol{g}| - 6\pi\eta R_{\mathrm{h}} u_y = 0 \tag{15b}$$

$$-6\pi\eta r_{\mathrm{h}} u_z = 0 \tag{15c}$$

$$u_x = 0 \tag{16a}$$

$$u_y = \frac{\left(m_{\mathrm{p}} M_{\mathrm{s}} L \left\{ \frac{m B_{\mathrm{r}}}{2\mu_0 k_{\mathrm{B}} T} \left[\frac{y+h}{\sqrt{(y+h)^2 + r^2}} - \frac{y}{\sqrt{y^2 + r^2}} \right] \right\} \times \frac{B_{\mathrm{r}} r^2}{2} \left[\frac{1}{\left[(y+h)^2 + r^2\right]^{\frac{3}{2}}} - \frac{1}{[y^2 + r^2]^{\frac{3}{2}}} \right] \right) - m_{\mathrm{p}}|\boldsymbol{g}|}{6\pi\eta R_{\mathrm{h}}} \tag{16b}$$

$$u_z = 0 \tag{16c}$$

3.2 Hydrodynamically interacting magnetophoresis model

In the previous model, the fluid is assumed to be stagnant and remains unaltered by the motion of the MNPs throughout the magnetophoresis process. In the second model, this assumption has been relaxed such that fluid flow could be generated within the MNPs solution due to MNPs/fluid interaction. Similar to the non MNPs/fluid interacting magnetophoresis model, the magnetophoresis of MNPs is also governed by the drift-diffusion equation stated in eqn (2). However in the hydrodynamically interacting magnetophoresis model, the momentum obtained by MNPs, which is due to the response of magnetic dipoles to the external magnetic field, is allowed to be transferred to the surrounding fluid as a consequence of the viscous property possessed by the fluid. Hence, eqn (16) are no longer valid in predicting the magnetophoretic velocity of MNPs. On the contrary, the convective motion of the MNPs solution is calculated by the well-known continuity and Navier–Stokes equations:[40]

$$\nabla \times u = 0 \tag{17}$$

$$\rho\left(\frac{\partial u}{\partial t} + u \times \nabla u\right) = -\nabla p + \eta \nabla^2 u + \rho \boldsymbol{g} + f_{\mathrm{m}} \tag{18}$$

By including the Navier–Stokes equation into this model, momentum transfer due to the MNPs/fluid interaction has been incorporated accordingly. eqn (17) and (18) govern the momentum transfer within the MNPs solution by connecting its spatial fluid flow profile to viscosity and external forces are imposed on it, namely, magnetic and gravitational forces. Besides, the MNPs solution is assumed to be an incompressible fluid, which is valid under atmospheric pressure. Herein, u is the velocity vector of the MNPs solution, ρ is the density of the MNPs solution, p is the absolute pressure and f_{m} is the volumetric magnetic force acting on the MNPs solution. The last term in eqn (18) represents the magnetic force acting on the unit volume of the MNPs solution due to the application of an external magnetic field. In other words, it is equivalent to the rate of momentum transfer into a unit volume of MNPs solution due to the collective response of this portion of solution to the external magnetic field. Therefore, f_{m} is a function of volumetric magnetization of MNPs solution, M, and magnetic flux density gradient, ∇B, which can be defined as follows:

$$f_{\mathrm{m}} = M \nabla B \tag{19}$$

Herein, the volumetric magnetization of the MNPs solution, M, is dependent on the concentration of MNPs, c, in the solution:

$$M = c M_{\mathrm{p,m}} \tag{20}$$

where $M_{\mathrm{p,m}}$ is mass magnetization of MNPs, as given in eqn (10). (Please refer to ESI,† S6 for details of computer simulation, including initial and boundary conditions employed in this model).

4 Results and discussion

4.1 Characterization of magnetic nanoparticles (MNPs)

Based on the image analysis performed on 136 MNPs captured by transmission electron microscopy, the average core size was determined to be 30.94 ± 2.18 nm. In addition, it can be observed that the MNPs were almost spherical in shape (Fig. 2a). Nevertheless, the average MNPs hydrodynamic diameter was measured using dynamic light scattering (DLS) (Malvern Instruments Nanosizer ZS), which was determined to be 43 nm; this value is roughly 12 nm larger than their particle core size due to the PEG coating (Fig. 2b).[35] The non-hysteretic behavior of the magnetization curve, which was recorded using a vibrating sample magnetometer (VSM) (ARkival ADE/DMS Model 880) measurements, clearly indicates the superparamagnetic nature of these MNPs with their saturation magnetization at 42.7 emu g^{-1} (Fig. 2c).[38]

4.2 Magnetophoresis kinetics profile

Under the influence of an external magnetic field generated by a grade N50 NdFeB cylindrical permanent magnet (1.4 cm in diameter and 1.5 cm in length) with the remanent magnetization of 1.45 T, suspended MNPs were attracted towards the bottom of the solution by the magnetic force, which decreased the MNPs concentration in the solution in tandem with the progression of time (Fig. 1). Fig. 3a illustrates that the normalized separation

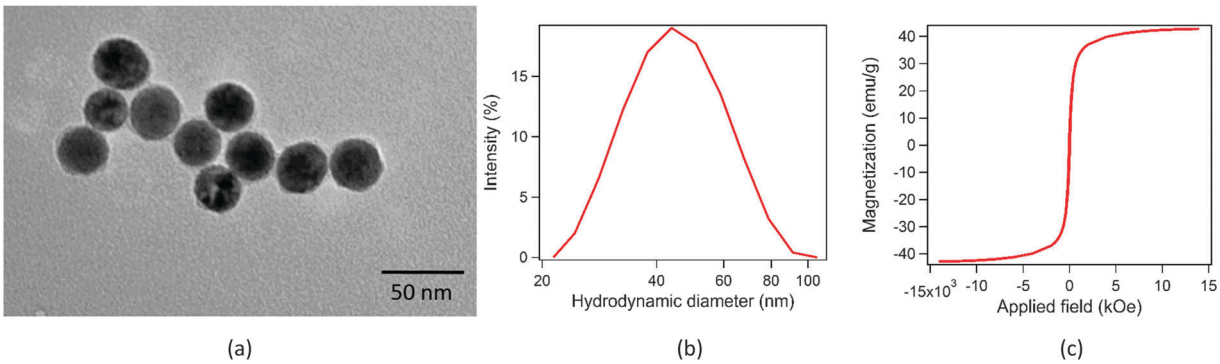

Fig. 2 (a) Transmission electron micrograph (TEM) of the MNPs. It can be observed that the MNPs are nearly spherical and their magnetic core size is approximately 30 nm. This result justifies the information provided by the supplier. The layer of PEG coating that surrounds MNPs is also noticeable. The aggregation of MNPs shown in this figure is due to the drying of the MNPs solution on the carbon grid prior to the TEM analysis. (b) Hydrodynamic size distribution of MNPs in the solution provided by DLS measurement. (c) Magnetization curve of MNPs used in this study.

kinetic profiles of the MNPs solution almost collapse into a single curve, regardless of the initial particle concentration used. This observation revealed that concentration effects, namely, MNPs/MNPs interaction, are insignificant in controlling the kinetics of magnetophoresis under LGMS. Rationally, the MNPs/MNPs interaction is more intense in highly concentrated MNPs solutions due to higher collision frequency, which subsequently leads to the formation of larger aggregates within a shorter period. Larger aggregates should be more magnetically responsive, and hence achieve a higher magnetophoretic velocity and accelerate the collection of MNPs under magnetophoresis.[19,20,26] Such concentration dependency of the separation kinetic profile has been observed in our previous study, in which intensively interacting MNPs systems were used.[41,42] However, the independence of the separation kinetic profile on MNPs concentration (Fig. 3a) leads us to deduce that the MNPs concentration range employed in this study (10–100 mg L^{-1}) is still far below the critical MNPs concentration in which interparticle interactions start to become significant. In addition, according to the theory developed by Andreu and coworkers,[24] magnetic interaction between MNPs is relevant only when the aggregation parameter, N^*, is larger than unity. For instance, the largest value of N^* considered in this study is given by 0.158 when the MNPs solution with a concentration of 100 mg L^{-1} was used (see ESI,† S3 for full details of the calculation). The aggregation parameter, N^*, should be much lower than this value in other cases in which the particle concentration is below 100 mg L^{-1}. Because the N^* values are well below unity within the concentration range (10–100 mg L^{-1}) considered in the current study, it can be concluded that magnetic interaction between MNPs and reversible aggregation is negligible. Because the ultimate goal of this study is to study the nature of the MNPs/fluid interaction under LGMS, this MNPs system is ideal and well-suited for the current investigation due to the fact that the MNPs/MNPs interaction is negligible and can be excluded.

Coincidentally, separation kinetic profiles measured at different locations throughout the MNPs solution also collapsed into a single curve (Fig. 3b). This observation indicates that the MNPs were uniformly distributed throughout the MNPs solution during the real time magnetophoresis process because the MNPs concentrations at different locations in the solution are similar within the entire time scale of the experiment. Under this circumstance, the

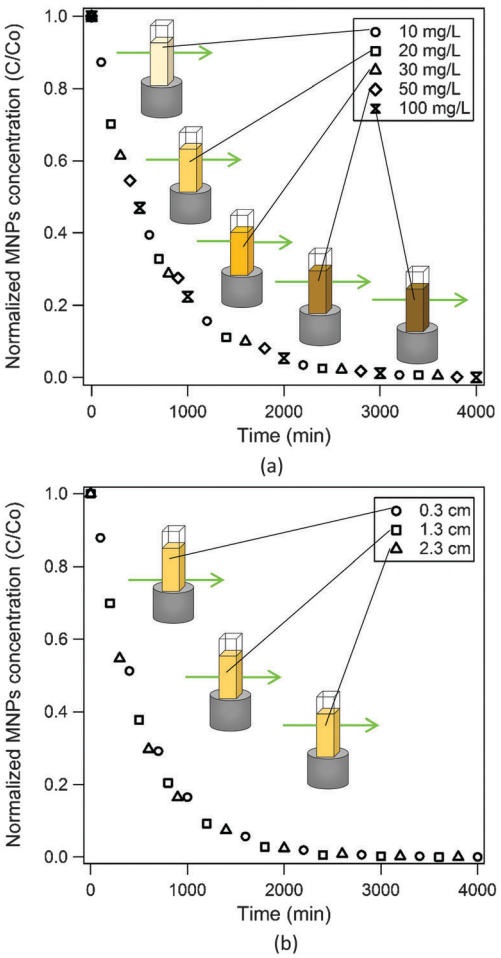

Fig. 3 (a) Separation kinetic profiles for experiments that employ MNPs solutions with different initial concentrations (ranging from 10 to 100 mg L^{-1}). The measurement was carried out at a position that was vertically 2.3 cm away from the bottom of the MNPs solution. (b) Separation kinetic profiles at different vertical positions (0.3, 1.3 and 2.3 cm from the bottom of the MNPs solution). 20 mg L^{-1} MNPs solution was used in this experiment.

MNPs solution in the cuvette remains homogeneous while undergoing magnetophoresis. The time-lapse images captured while the MNPs solution was undergoing magnetophoresis (Fig. 4) further verify this argument. This experimental observation provides the first evidence, which suggests the importance of the hydrodynamic effect associated to magnetophoresis; this is the subject of discussion in the following sections.

4.3 Non MNPs/fluid interacting magnetophoresis

As shown in the time lapse images of the simulation results in Fig. 5a, the non MNPs/fluid interacting model predicted progressive clearing of MNPs at the bottom of the cuvette, where the magnetic flux density gradient is the highest. Rationally, the simulation result displays this behavior because of the spatial resolution of the magnetic flux density gradient from the magnet pole,[43] which causes the MNPs that are located closer to the magnet to experience a much greater magnetophoretic force and hence migrate at a faster speed to the magnetic source compared to those located further away from the magnet.[15] For instance, an MNP with a diameter of 30 nm located 1 mm away from the magnet pole face experiences the magnetic flux density gradient ∇B of 93.8 T m^{-1}, which corresponds to a magnetophoretic force of 0.203 fN. In comparison, the same particle experiences considerably weaker magnetophoretic force of 0.038 fN as the separation distance from the magnet pole face increases to 10 mm with magnetic flux density gradient of 17.5 T m^{-1}. Therefore, MNPs that experience a greater magnetophoretic force will move at a higher speed, and thus can be captured and separated from the solution much quickly. Under this scenario, MNPs at the bottom portion of the solution are collected from the aqueous environment much more rapidly as magnetophoresis begins, which is expected to create a particle concentration gradient across the suspension from the bottom (high ∇B) to the top (low ∇B). In fact, this phenomenon is further amplified by the MNPs/MNPs interaction and is well aligned with our previous experimental observation for an intensively MNPs/MNPs interacting system.[41] On a side note, this result serves as the best indication in which the continuous homogenization of the MNPs suspension is not related to the MNPs/MNPs interaction.

However, the non MNPs/fluid interacting magnetophoresis model simulation result contradicts the experimental observation, which displays homogeneity throughout the MNPs solution the entire time, as described in the previous section. As a consequence, there exists a huge discrepancy between the magnetophoresis separation kinetic profiles obtained from experiment and predicted by the non MNPs/fluid interacting magnetophoresis model (Fig. 5b). The two major differences between the experimental and simulation results are as follows: (1) MNPs were always homogeneously distributed throughout the whole solution in the experiment (Fig. 3b and 4), while apparent non-uniformity was observed in the model simulation result, which is implied by the location dependency of the separation kinetic profile (Fig. 5a and b) and (2) MNPs collection time predicted by simulation was considerably longer compared to the experimental result. This peculiar observation indicates the failure of the classical non MNPs/fluid interacting magnetophoresis model in predicting the separation kinetic profile for our model system.

The homogeneity of the MNPs solution demonstrates that there is a driving force that distributes the MNPs throughout the solution during magnetophoresis. This driving force is probably contributed by fluid convection, which is usually portrayed as a vital role in the agitation or mixing of a solution. Because the surrounding fluid is non-magnetically responsive, it must obtain momentum from the MNPs motion to initiate convection under magnetophoresis. Therefore, there should be some type of interaction between MNPs and fluid (hydrodynamic interaction) so that momentum from the moving MNPs can be transferred to the surrounding fluid and lead to the occurrence of convection. Subsequently, this finding has led us to believe hydrodynamic effects, which originate from the MNPs/fluid interaction, might be the predominating factor in homogenizing the MNPs suspension and later accelerate the magnetophoretic capture of the MNPs.

4.4 Magnetophoresis induced convection

The dye-tracing experiment was conducted to trace the fluid motion in the MNPs solution, while it is undergoing magnetophoresis. A control experiment was also conducted using a blank solution (with 0 mg L^{-1} of MNPs). It was observed that for the control experiment the injected dye at the bottom of the solution diffused slowly and gradually filled up the whole solution due to thermal energy without any occurrence of magnetophoresis.[44] For all the other MNPs solutions, the dye moved upward relatively fast and filled up the solution at a much more rapid pace under magnetophoresis (Fig. 6). The instantaneous migration of the dye in the MNPs solution after its exposure to an external magnetic field further indicates that convection is generated in the MNPs solution during magnetophoresis. This convective flow induces mixing process and further enhances the dispersion of MNPs inside the solution and homogenized the suspension, as observed in the experiment described in the previous sections (Fig. 3b and 4). In addition, as depicted in Fig. 6, dye homogenization is more rapid when the MNPs concentration is higher as a result of stronger convective flux under magnetophoresis. Moreover, the decline in the standard deviation of light intensity throughout the MNPs solution, as shown in Fig. 7, further confirmed the homogenization of the solution as time progresses. Moreover, it can be observed that dye homogenization rate (which is equivalent to the rate of decay of the

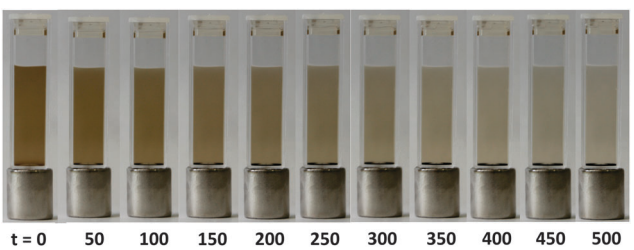

Fig. 4 Time lapse images of MNPs solution captured in real time experiment. The unit of time, *t*, is minutes.

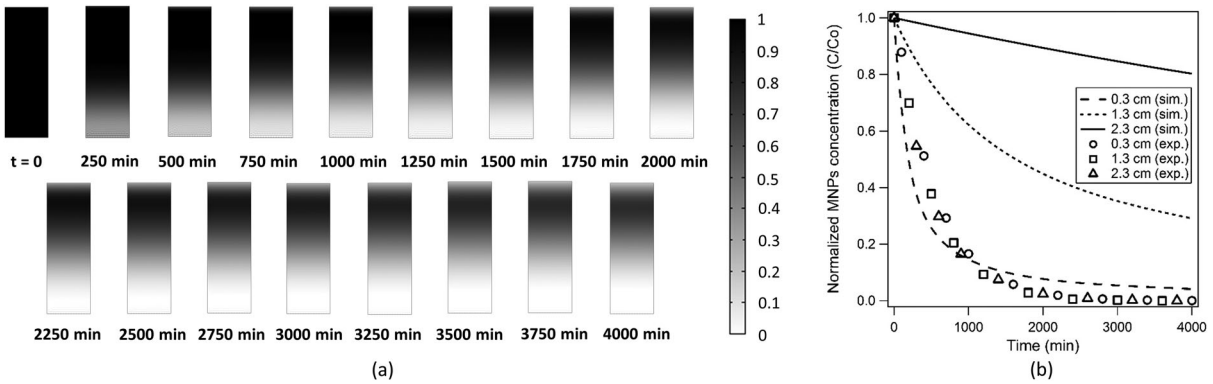

Fig. 5 (a) Time lapse images of MNPs solution generated by non MNPs/fluid interacting magnetophoresis simulation for the first 500 minutes after being subjected to magnetophoresis. The model simulation was carried out using COMSOL Multiphysics. The color bar indicates the normalized MNPs concentration in the surface plots of the MNPs solution, which range from 0 (MNPs concentration is zero) to 1 (initial MNPs concentration before subjecting to magnetophoresis). (b) Comparison between the separation kinetic profiles simulated by COMSOL Multiphysics according to the non MNPs/fluid interacting magnetophoresis model (sim.) and obtained from experiment (exp.) at different vertical positions along the cuvette.

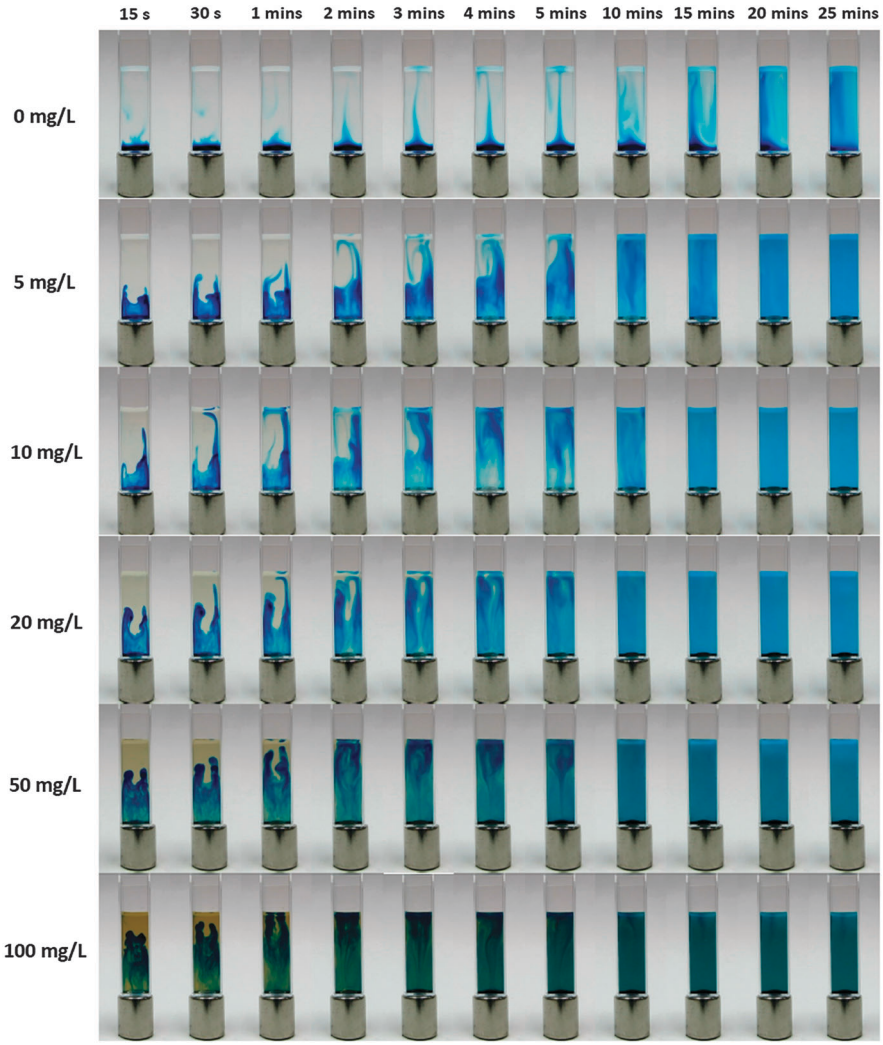

Fig. 6 Time lapse images for MNPs solution, which has been injected with 3000 mg L^{-1} of MB, with different concentrations (ranging from 0 to 100 mg L^{-1}) for the first 25 minutes after being subjected to magnetophoresis. The images in the first row illustrate the dye motion within a blank solution exposed to an external magnetic field, which was used as the controlled experiment.

light intensity standard deviation) increases with the concentration of MNPs solution. Therefore, according to this analysis, convection is more vigorous in more concentrated MNPs solution that is undergoing magnetophoresis, which is consistent with the time lapse images displayed in Fig. 6. Based on this observation, it can be deduced that convective motion, which occurs during the magnetophoresis of MNPs, is also dependent on the concentration of MNPs. This unique feature of magnetophoresis, in which fluid convection is induced as a consequence of the MNPs/fluid interaction throughout the process, is not well documented and is the focus of the following discussion.

Macroscopically, the occurrence of fluid convection during the magnetophoresis of a MNPs solution can be rationalized using the magnetic buoyancy concept. Magnetic buoyancy is defined as force exerted on an object that is immersed in a fluid, in which the surrounding fluid has higher volumetric magnetization compared to the object itself, under an externally applied magnetic field (Fig. 8a).[45] This magnetic buoyancy concept has been demonstrated by the migration of non-magnetic particles, which are immersed in an MNPs solution, in the opposite direction to the magnetic source (magnet) when the MNPs solution is subjected to magnetophoresis.[46,47] By taking the underlying principle of buoyancy as a reference, there is an analogy that can be drawn between the natural convection of a fluid above a horizontal heating plate and magnetophoresis of MNPs under our experiment conditions (Table 1). When a fluid is in thermal contact with a hot horizontal plate, the temperature of the fluid layer in the vicinity of the contacted surface increases, and the fluid becomes less dense and experiences lower gravitational force per unit volume compared to the surrounding fluid. Thus, the bottom layer of the fluid is driven upwards by the gravitational buoyancy force. As the hot fluid with less density moves upward, the cooler fluid at the top moves down to replace it and complete the flow cycle, which causes convectively driven fluid circulation. Likewise, the convective flow in the magnetophoresis of a MNPs solution can also be explained in a similar manner. Because MNPs tend to be attracted towards the region with higher magnetic flux density, MNPs at the bottom of the solution are continuously depleted (captured on the cuvette wall) due to magnetophoretic collection. This condition causes a temporary decline in the MNPs concentration and hence reduction of volumetric magnetization of the bottom portion of the solution. Consequently, the magnetic force per unit volume experienced by this portion of MNPs solution is relatively lower compared to that of the upper portion of the MNPs solution.[39] Therefore, the MNPs solution with lower volumetric magnetization is driven upwards by magnetic buoyancy force so that the fluid at the upper portion moves down to replace it. In this way convective current is generated in the MNPs solution during magnetophoresis, which is consistent with the experimental observation (Fig. 6). This scenario is in fact the driving mechanism for continuous homogenization of the solution, which causes the uniform distribution of MNPs as magnetophoresis proceeds (Fig. 4).

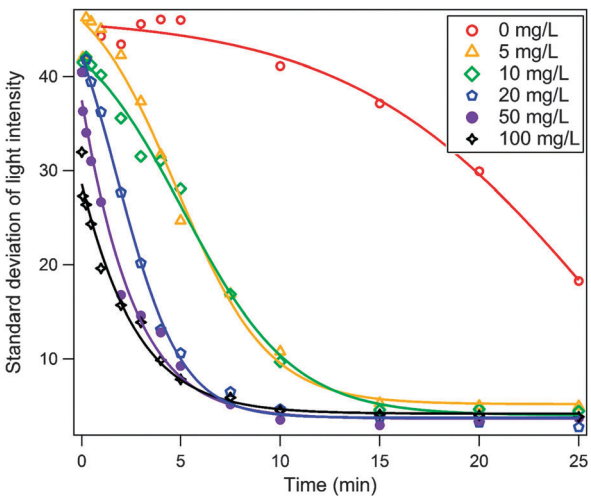

Fig. 7 Evolution of light intensity standard deviation throughout the MNPs solution (calculated from about 85 000 pixels) with time. The image analysis was performed using ImageJ. The lower the light intensity standard deviation, the smaller the dispersion of light intensity and hence the more uniform the dye distribution in the MNPs solution. Continuous lines are inserted to guide the eyes.

In conjunction with the case of natural convection, the significance of magnetophoresis induced convection is dictated by magnetic buoyancy and viscous force. To have a better quantitative characterization of these two forces under the context of magnetophoresis induced convection, a new concept known as the magnetic Grashof number, Gr_m, is introduced. Conventionally, the Grashof number is a dimensionless number used to represent the ratio of the buoyancy force to viscous force in a natural convective flow system, which is given as follows:[48]

$$Gr = \frac{|\boldsymbol{g}|\frac{1}{V}\left(\frac{\partial V}{\partial T}\right)_P (T_s - T_\infty) {L_c}^3}{\nu^2} \quad (21)$$

where V is volume per unit mass, T_s is the temperature of the heating plate, T_∞ is the bulk temperature of the fluid, L_c is the characteristic length and ν is the kinematic viscosity of the fluid. To analogously define the Grashof number in the magnetophoresis system, the classical Grashof number for a natural convection system was classified into five parts: (1) force (gravitational force) experienced by a unit mass of fluid under a force field (gravitational field), (2) fractional change of fluid property (volume per unit mass) with respect to another fluid property (temperature), which induces the buoyancy effect on the fluid, (3) driving force for transportation, (4) characteristic length and (5) kinematic viscosity of fluid. Table 2 shows a breakdown of the Grashof number as stated above. Likewise, the magnetic Grashof number, Gr_m, is analogously defined according to the five parts of the Grashof number division as listed in the third column of Table 2. Therefore, Gr_m is given as follows:

$$Gr_m = \frac{\nabla B\left(\frac{\partial M}{\partial c}\right)_H (c_s - c_\infty) {L_c}^3}{\rho \nu^2} \quad (22)$$

where M is magnetization per unit mass of MNPs solution, c is concentration of MNPs solution, c_s is MNPs concentration of the surface adjacent to the magnet, c_∞ is bulk MNPs concentration

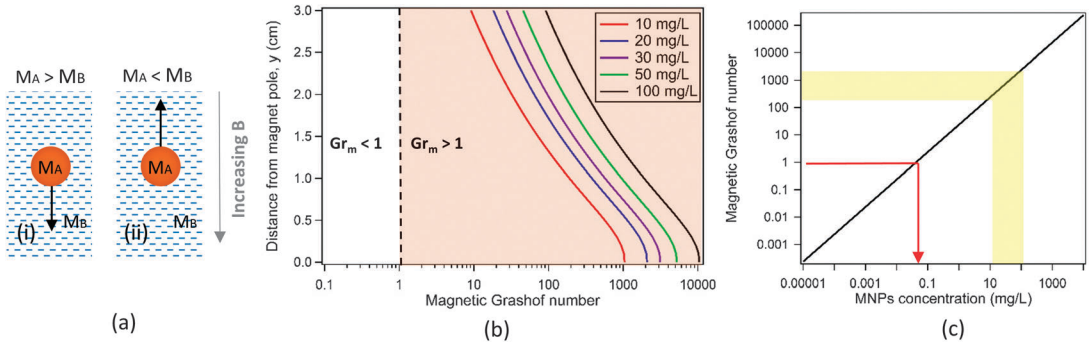

Fig. 8 (a) (i) When a more magnetically responsive object immersed in a fluid with lower volumetric magnetization is exposed to an external magnetic field, the object will be driven to the region where magnetic flux density is higher. (ii) In contrast, if the surrounding fluid is more magnetically responsive than the immersed object, the object will experience a negative magnetic force which drives it to a region where the magnetic flux density is relatively lower. This opposite force is generally known as magnetic buoyancy. (b) The plot of distance from magnet pole against magnetic Grashof number of MNPs solution at different MNPs concentrations. The magnetic Grashof number is calculated according to the experimental configuration in the current study. (c) The graph of magnetic Grashof number against MNPs concentration. The calculation was done by adopting the average magnetic flux density gradient in the experimental setup illustrated in Fig. 1. Magnetic Grashof number can only be less than unity provided the concentration of MNPs solution is below 0.05 mg L^{-1} (red arrow).

Table 1 Analogous comparison between natural convection and magnetophoresis

Process	Illustration	'Substance' to be transferred	Type of field	Driving force	Fluid property which induces convection
Natural convection	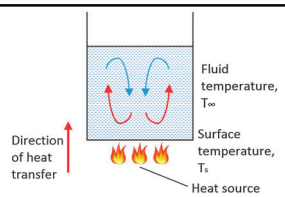	Heat energy	Gravitational field	Temperature gradient	Volume per unit mass
Magnetophoresis	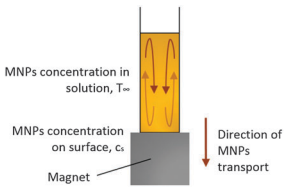	MNPs	Magnetic field	Concentration gradient	Magnetization per unit mass

of the MNPs solution, L_c is characteristic length, ρ is density of MNPs solution and ν is kinematic viscosity of the MNPs solution. The magnetophoresis induced convection is noteworthy if Gr_m is larger than unity.

Because Gr_m is a function of ∇B, its magnitude decreases with respect to the separation distance from the magnet pole due to the rapid decay of ∇B (Fig. 8b). However, even at the very low MNPs concentration of 10 mg L^{-1}, the Gr_m of the solution is still greater than unity. This is because magnetophoresis induced convection is inevitable and serves as a critical element, which influences the dynamic behavior of the magnetophoresis process in this experiment. According to eqn (17), it is apparent that Gr_m is also dependent on the concentration of the MNPs solution subjected to magnetophoresis (Fig. 8c). With a higher Gr_m value, the convective flow becomes more vigorous in a concentrated MNPs solution and this analysis is consistent with our experimental observation, as indicated in Fig. 6 and 7. Furthermore, according to our calculation, Gr_m is less than unity only when the MNPs concentration is smaller than 0.05 mg L^{-1}. However, this concentration is too low to be useful for any engineering practical purpose. Therefore, magnetophoresis induced convection will always be significant for any type of engineering application that involves LGMS.

Table 2 Breakdown of the classical Grashof number into five parts in order to facilitate the analogous derivation of the magnetic Grashof number

Part	Natural convection	Magnetophoresis
1	$\lvert g\rvert$	$\frac{M\nabla B}{\rho}$
2	$\frac{1}{V}\left(\frac{\partial V}{\partial T}\right)_P$	$\frac{1}{M}\left(\frac{\partial M}{\partial c}\right)_H$
3	$T_s - T_\infty$	$c_s - c_\infty$
4	L_c	L_c
5	ν	ν

4.5 Hydrodynamically interacting magnetophoresis model

Magnetophoresis induced convection demonstrates the significance of the MNPs/fluid interaction in governing the transport

behavior of MNPs under a magnetic field. This is the main reason for the failure of the non MNPs/fluid interacting magnetophoresis model to describe the real time magnetophoresis process precisely. Consequently, the hydrodynamically interacting magnetophoresis model, which takes the MNPs/fluid interaction into consideration, was developed (Section 3.2) to predict the separation kinetic profile of a MNPs solution undergoing low gradient magnetophoresis. Indeed, the simulation result from this model shows good agreement with the experimental observation (Fig. 9a), which implies the significance of the MNPs/fluid interaction throughout LGMS. There are two important features that can be noticed from the simulation result of the hydrodynamically interacting magnetophoresis model. The first feature is the uniform distribution of MNPs throughout the entire solution during magnetophoresis, regardless at which position the MNPs concentration is recorded (Fig. 9b). This simulation results is consistent with our previous experiment, which shows a constant separation kinetic profile with respect to spatial distribution in Fig. 3b. For instance, according to the simulation result from the non MNPs/fluid interacting magnetophoresis model, 500 minutes after the magnetophoresis started, the normalized MNPs concentration is given by 0.2522, 0.7531 and 0.9546 at the positions with the vertical distance of 4 mm, 13 mm and 23 mm from the magnet pole, respectively. On the contrary, the hydrodynamically interacting magnetophoresis model predicts that the normalized MNPs concentration is given by 0.4748, 0.4643 and 0.4705 at the three given positions at the same moment. These values are close to each other and this indicates that the MNPs are almost uniformly distributed throughout the whole solution. The second feature is the occurrence of convective flow in the MNPs solution during the magnetophoresis process (Fig. 9c) and its convective rate is dependent upon particle concentration. According to our simulation result, convective flow ranging from 10^{-5} to 10^{-4} m s^{-1} is induced in the magnetophoresis of a MNPs solution with the concentration of 10 mg L^{-1}. The occurrence of induced convective flow indicates that the fluid possesses momentum throughout magnetophoresis. For instance, the momentum in this system originates from the magnetic force that is acting upon the MNPs suspended in the solution under an external magnetic field. Due to the viscous property of the surrounding fluid, momentum is transferred to it when a velocity gradient is present in the solution and the fluid starts to flow. The two important features mentioned above are observed in our experiment, as described in the previous sections. The agreement between our experiment and simulation

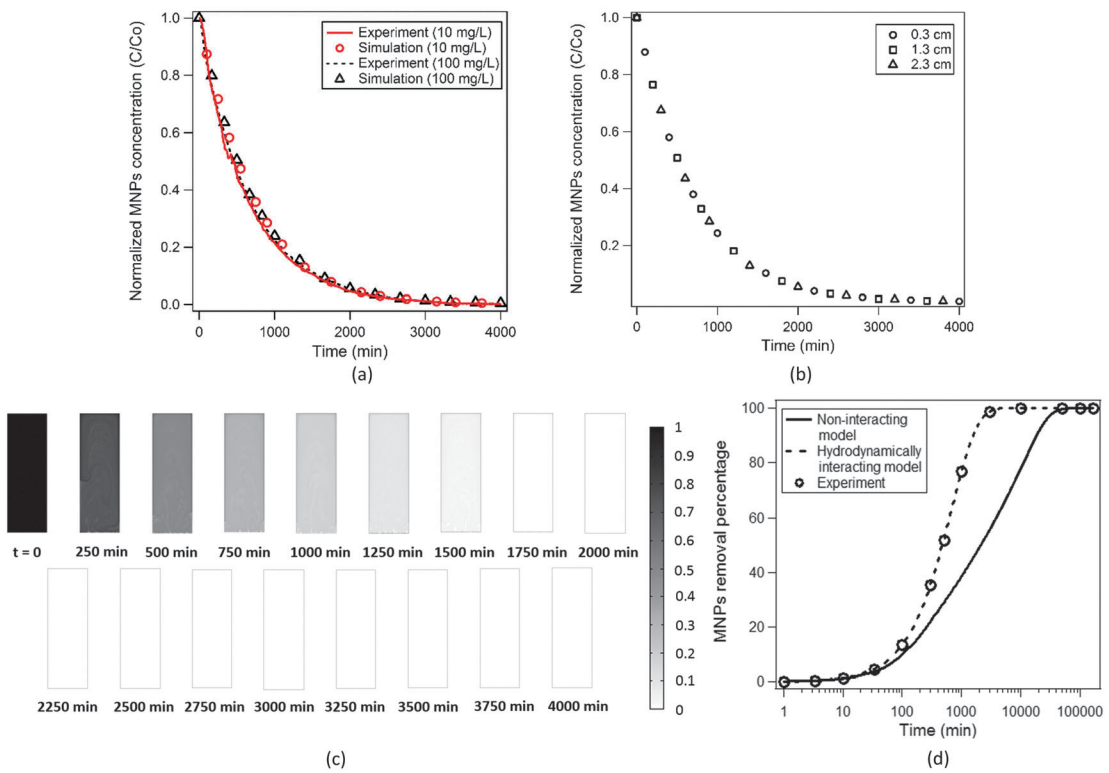

Fig. 9 (a) Comparison between experimental and simulation result. The simulation result is generated by COMSOL Multiphysics according to the hydrodynamically interacting magnetophoresis model. The normalized MNPs concentration is probed at a position that is vertically 2.3 cm away from the magnet pole. (b) Comparison between separation kinetic profiles (predicted from simulation of the hydrodynamically interacting magnetophoresis model) at three different locations of the MNPs solution where vertical distances from the magnet pole are given by 0.3 cm, 1.3 cm and 2.3 cm. Initial MNPs concentration of 10 mg L^{-1} is adopted in this simulation. (c) Time lapse images of MNPs solution generated by COMSOL Multiphysics based on the simulation result from the hydrodynamically interacting magnetophoresis model. The color bar indicates the normalized MNPs concentration in the surface plots of the MNPs solution. (d) Comparison between MNPs removal profile predicted by the non MNPs/fluid interacting magnetophoresis model and hydrodynamically interacting magnetophoresis model. The experimental result agrees with the simulation result from the hydrodynamically interacting magnetophoresis model.

results confirms the importance of the MNPs/fluid interaction in controlling the LGMS performance.

Apart from this, it is desirable to study the effect of the MNPs/fluid interaction on the magnetophoretic capture rate of MNPs during low magnetic field gradient magnetophoresis. As shown in Fig. 9d, it can be observed that the induced convection accelerates the magnetophoretic collection rate of MNPs (hydrodynamically interacting magnetophoresis model) in comparison to the system in which the surrounding fluid remains stagnant (non MNPs/fluid interacting magnetophoresis model). Based on the simulation result from the non MNPs/fluid interacting magnetophoresis model, approximately 85 000 minutes is required to achieve 99% of MNPs removal. In contrast, the separation time is greatly reduced to 3100 minutes, according to the simulation result from the hydrodynamically interacting magnetophoresis model, which is about 27 times faster compared to the result predicted by the non MNPs/fluid interacting magnetophoresis model. The rapid magnetophoretic capture rate is mainly due to the continuous sweeping of the MNPs that are located far from the magnet, where ∇B is relatively lower, to the region closer to the magnet; at this point it experiences a much stronger magnetic force by magnetophoresis induced convection and the MNPs are separated from the solution within a shorter time scale. In this way, the MNPs/fluid interaction greatly alters the dynamic behavior of magnetophoresis, accelerates the magnetic separation process and improves the practicability of LGMS in engineering applications.

5 Conclusion

We have revealed the pivotal role of the sweeping flow created from MNPs convection in self-dispersing MNPs during the magnetophoresis process. Even in an extremely diluted MNPs solution, with the concentration of 10 mg L^{-1}, in which MNPs/MNPs interaction is negligible, this hydrodynamic driven phenomenon is still nontrivial. The continuous dispersion of MNPs into the suspension leads to the homogenous distribution of MNPs across the entire solution and greatly influences the dynamic behavior of LGMS. One of the most significant advantages contributed by the MNPs/fluid interaction to LGMS is the rapid magnetophoretic capture of MNPs during magnetophoresis. We believe by taking advantage of this scenario, it is possible to overcome one of the most significant problems in implementing LGMS for large scale engineering applications, which is the extremely rapid decay of ∇B with distance from the magnet that leads to the poor separation performance of LGMS.[43] In the case of cooperative magnetophoresis (under the MNPs/MNPs interacting mode),[22] we anticipated that the influence of the hydrodynamic effect is dependent on MNPs concentration. At moderate to high MNPs concentrations, magnetophoresis induced convection creates agitation within the MNPs solution and enhances the mixing of MNPs, which in turn promotes the acceleration of MNP aggregation and magnetophoretic separation. For extreme cases with extremely high MNPs concentrations, we anticipated that 'cooperative factors' would overwhelm the hydrodynamic effects mainly due to the (1) high aggregation kinetic of MNPs and (2) larger MNPs cluster size formed, which leads to fast motion of the cluster under magnetophoresis. In conclusion, the MNPs/fluid interaction (which is generally known as the hydrodynamic interaction) is the influential fundamental interaction that controls the magnetophoretic behavior of a MNPs solution that is undergoing magnetophoresis and it should be taken into consideration in the modeling of the magnetophoresis process and design of magnetic separators.

Acknowledgements

Sim Siong Leong acknowledges the support from the Ministry of Higher Education of Malaysia through the MyPhD Scholarship. This project was also financially supported by Research University grant from USM (Grant no. 1001/PJKIMIA/811219) and FRGS grant from MOHE (Grant no. 203/PJKIMIA/6071269). We gratefully acknowledge Prof. Tim St Pierre from University of Western Australia for the discussion on magnetic buoyancy force.

References

1 Q. A. Pankhurst, J. Connolly, S. K. Jones and J. Dobson, *J. Phys. D: Appl. Phys.*, 2003, **36**, R167.
2 A. K. Gupta and M. Gupta, *Biomaterials*, 2005, **26**, 3995–4021.
3 J. Dobson, *Gene Ther.*, 0000, **13**, 283–287.
4 W. H. De Jong and P. J. A. Borm, *Int. J. Nanomed.*, 2008, **3**, 133–149.
5 K. E. McCloskey, J. J. Chalmers and M. Zborowski, *Anal. Chem.*, 2003, **75**, 6868–6874.
6 M. Zborowski and J. J. Chalmers, *Anal. Chem.*, 2011, **83**, 8050–8056.
7 C. T. Yavuz, A. Prakash, J. T. Mayo and V. L. Colvin, *Chem. Eng. Sci.*, 2009, **64**, 2510–2521.
8 Y. F. Shen, J. Tang, Z. H. Nie, Y. D. Wang, Y. Ren and L. Zuo, *Sep. Purif. Technol.*, 2009, **68**, 312–319.
9 I. Akin, G. Arslan, A. Tor, M. Ersoz and Y. Cengeloglu, *J. Hazard. Mater.*, 2012, **235–236**, 62–68.
10 P. Xu, G. M. Zeng, D. L. Huang, C. L. Feng, S. Hu, M. H. Zhao, C. Lai, Z. Wei, C. Huang, G. X. Xie and Z. F. Liu, *Sci. Total Environ.*, 2012, **424**, 1–10.
11 S. C. N. Tang and I. M. C. Lo, *Water Res.*, 2013, **47**, 2613–2632.
12 V. Schaller, U. Kräling, C. Rusu, K. Petersson, J. Wipenmyr, A. Krozer, G. Wahnström, A. Sanz-Velasco, P. Enoksson and C. Johansson, *J. Appl. Phys.*, 2008, **104**, 093918.
13 A. F. Pshenichnikov and A. S. Ivanov, *Phys. Rev. E: Stat., Nonlinear, Soft Matter Phys.*, 2012, **86**, 051401.
14 J. Gómez-Pastora, E. Bringas and I. Ortiz, *Chem. Eng. J.*, 2014, **256**, 187–204.
15 J. Lim, C. Lanni, E. R. Evarts, F. Lanni, R. D. Tilton and S. A. Majetich, *ACS Nano*, 2010, **5**, 217–226.
16 G. D. Moeser, K. A. Roach, W. H. Green, T. Alan Hatton and P. E. Laibinis, *AIChE J.*, 2004, **50**, 2835–2848.
17 P. Y. Toh, S. P. Yeap, L. P. Kong, B. W. Ng, D. J. C. Chan, A. L. Ahmad and J. K. Lim, *Chem. Eng. J.*, 2012, **211–212**, 22–30.

18 G. Mariani, M. Fabbri, F. Negrini and P. L. Ribani, *Sep. Purif. Technol.*, 2010, **72**, 147–155.
19 C. T. Yavuz, J. T. Mayo, W. W. Yu, A. Prakash, J. C. Falkner, S. Yean, L. Cong, H. J. Shipley, A. Kan, M. Tomson, D. Natelson and V. L. Colvin, *Science*, 2006, **314**, 964–967.
20 G. De Las Cuevas, J. Faraudo and J. Camacho, *J. Phys. Chem. C*, 2008, **112**, 945–950.
21 L. E. Helseth and T. Skodvin, *Meas. Sci. Technol.*, 2009, **20**, 095202.
22 J. Faraudo and J. Camacho, *Colloid Polym. Sci.*, 2010, **288**, 207–215.
23 J. S. Andreu, J. Camacho, J. Faraudo, M. Benelmekki, C. Rebollo and L. M. Martínez, *Phys. Rev. E: Stat., Nonlinear, Soft Matter Phys.*, 2011, **84**, 021402.
24 J. S. Andreu, J. Camacho and J. Faraudo, *Soft Matter*, 2011, **7**, 2336–2339.
25 J. S. Andreu, P. Barbero, J. Camacho and J. Faraudo, *J. Nanomater.*, 2012, **2012**, 5.
26 J. Faraudo, J. S. Andreu and J. Camacho, *Soft Matter*, 2013, **9**, 6654–6664.
27 Y. Xu, Y. Qin, S. Palchoudhury and Y. Bao, *Langmuir*, 2011, **27**, 8990–8997.
28 R. Lakshmanan, C. Okoli, M. Boutonnet, S. Järås and G. K. Rajarao, *Bioresour. Technol.*, 2013, **129**, 612–615.
29 R. Lakshmanan, M. Sanchez-Dominguez, J. A. Matutes-Aquino, S. Wennmalm and G. Kuttuva Rajarao, *Langmuir*, 2014, **30**, 1036–1044.
30 S. A. Khashan, E. Elnajjar and Y. Haik, *J. Magn. Magn. Mater.*, 2011, **323**, 2960–2967.
31 S. A. Khashan and E. P. Furlani, *Microfluid. Nanofluid.*, 2012, **12**, 565–580.
32 S. A. Khashan and E. P. Furlani, *J. Phys. D: Appl. Phys.*, 2013, **46**, 125002.
33 S. A. Khashan and E. P. Furlani, *Sep. Purif. Technol.*, 2014, **125**, 311–318.
34 S. A. Khashan, A. Alazzam and E. P. Furlani, *Sci. Rep.*, 2014, **4**, 5299.
35 J. Lim, S. Yeap, H. Che and S. Low, *Nanoscale Res. Lett.*, 2013, **8**, 381.
36 Z. Zhang and J. Kong, *J. Hazard. Mater.*, 2011, **193**, 325–329.
37 E. P. Furlani and K. C. Ng, *Phys. Rev. E: Stat., Nonlinear, Soft Matter Phys.*, 2008, **77**, 061914.
38 G. P. Hatch and R. E. Stelter, *J. Magn. Magn. Mater.*, 2001, **225**, 262–276.
39 R. E. Rosensweig, *Ferrohydrodynamics*, Dover Publications, New York, 2014.
40 R. B. Bird, W. E. Stewart and E. N. Lightfoot, *Transport Phenomena*, Wiley, New York, 2006.
41 J. Lim, S. P. Yeap and S. C. Low, *Sep. Purif. Technol.*, 2014, **123**, 171–174.
42 S. P. Yeap, S. S. Leong, A. L. Ahmad, B. S. Ooi and J. Lim, *J. Phys. Chem. C*, 2014, **118**, 24042–24054.
43 J. Lim, S. P. Yeap and S. C. Low, *Sep. Purif. Technol.*, 2014, **123**, 171–174.
44 H. C. Berg, *Random Walks in Biology*, Princeton University Press, Chichester, 1993.
45 K. Henjes, *Z. Phys. B: Condens. Matter*, 1993, **92**, 113–127.
46 R. M. Erb, H. S. Son, B. Samanta, V. M. Rotello and B. B. Yellen, *Nature*, 2009, **457**, 999–1002.
47 M. Benelmekki, L. M. Martinez, J. S. Andreu, J. Camacho and J. Faraudo, *Soft Matter*, 2012, **8**, 6039–6047.
48 J. P. Holman, *Heat Transfer*, McGraw-Hill, New York, 2008.

